CHAPTER VI
GRAPHENE/GELATIN HYDROGEL COMPOSITES WITH HIGH STORAGE MODULUS SENSITIVITY FOR USING AS ACTUATOR: EFFECTS OF SURFACE AREA AND ELECTRIC FIELD STRENGTH

6.1 Abstract

The electromechanical properties of graphene/gelatin hydrogel composites were investigated under the effects of graphene surface areas, electric field strength and temperature towards bio-actuator applications. The highest surface area of an embedded graphene (MG; grade M) in the gelatin hydrogel composites induced the highest dynamic modulus (G') under applied electric field. The 0.1 vol% graphene (MG)/gelatin hydrogel composite possessed the highest $\Delta G'/G'_o$ value of 352 % in comparison with other materials in previous studies. Even the lowest $\Delta G'/G'_o$ values obtained from the fabricated graphene/hydrogel composites were still greater than other dielectric elastomer materials. The storage moduli of the pure gelatin and graphene (MG)/gelatin hydrogel composites, between 30 °C and 90 °C, exhibited three distinct regimes. In the deflection experiment, the bending distance and the dielectrophoresis force were found to increase monotonically with applied electric field strength with a deflection toward the anode side, indicating the attractive force between the anode and the polarized carboxyl group as the gelatin structure possessed negative charges.

Keywords: Electromechanical properties; Actuator; Biopolymer; Gelatin; Hydrogels; Graphene

6.2 Introduction

Electroactive polymers (EAPs) have been developed for many applications such as compliant electrode (Kujawski *et al.*, 2010), drug delivery engineering (Goenka *et al.*, 2014), actuator (Shiga, 1997), electroactive paper (Kim *et al.*, 2008), and many others (Bar-cohen, 2001) that offer distinct characteristics: high energy density, light weight, and great flexibility. Hydrogels are promising materials for development of EAPs because they provide a reversible response to external stimuli such as ionic strength (Miyata *et al.*, 1999; Kim *et al.*, 2002), pH (Tanaka *et al.*, 1980; Siegel *et al.*, 1988), temperature (Hoffman, 1987; Bae *et al.*, 1987; Okano *et al.*, 1990; Zareie *et al.*, 2000), and electric field (Tanaka *et al.*, 1982; Kwon *et al.*, 1991; Kim *et al.*, 2002; Tungkavet *et al.*, 2012). Gelatin is a hydrogel or EAP that has a high molecular weight protein produced from animal collagen by thermal and hydrolyzing processes with either acids or bases. It can be used as a stable film, hydrogel, and composite (Yang *et al.*, 1997). However, gelatin possesses poor water resistance and low mechanical properties because the oriented structure is split into a random coil structure after treating through acid or base at high temperature, these restrict its possible application as an EAP (Tungkavet *et al.*, 2011). Therefore, gelatin needs to be reinforced through either chemical crosslinking or use of filler materials. Chemical crosslinking enhances thermal and mechanical properties through covalent bonds between the reactive side groups in the gelatin molecules. However, this process produces the residual crosslinking agents, leading to the toxic side effects. The use of graphene embedded in gelatin has been studied by Wang *et al.* (2012). They found that graphene/gelatin gel composites exhibit high tensile strength compared with pure gelatin films in both dry and wet states. Zhang *et al.* (2011) investigated thermal and mechanical properties of sodium alginate/graphene oxide composites. Graphene oxide (GO) enhanced the stability of sodium alginate without crosslinking chemicals because of dispersion and compatibility of GO in the polymer matrix. Graphene, one of the elementary carbon structures (fullerene, diamond, carbon nanotube), is a single atom layer of carbon that is arranged in a two dimensional monolayer (Ionita *et al.*, 2013). It has promising properties, including high electrical conductivity at ambient temperature (Novoselov *et al.*, 2004), good

thermal conductivity (Balandin *et al.*, 2008), large surface area, and outstanding mechanical properties in term of Young's modulus (Lee *et al.*, 2008). Compared with diamond, fullerene, and carbon nanotubes (CNTs), graphene is much easier to obtain and at a lower price. Thus, graphene is a suitable carbon based reinforcement filler used for enhancing mechanical performance of polymer matrix (Liang *et al.*, 2009). For example, Liang *et al.* (2009) studied graphene/PVA nanocomposite that used graphene as a reinforcement filler. Tensile strength and young's modulus were increased by 76 % and 62 %, respectively when compared with neat PVA through the distribution of 0.7 %wt GO. Therefore, graphene is an excellent-reinforcing material for polymers that have been developed for several applications such as electronic and optoelectronic devices, bio-chemical sensors, nanocomposites, and energy storage (Singh *et al.*, 2011).

The objective of present work was to investigate the electromechanical properties of graphene/gelatin hydrogel composites containing an anionic surfactant (i.e., sodium dodecylsulfate) as candidate materials for bio–actuator applications. The electrical, thermal, and electromechanical properties were investigated and measured under the influences of graphene content and surface area, electric field strength, and temperature.

6.3 Experimental

6.3.1 Materials

Gelatin (Type B, bovine skin) and sodium dodecyl sulfate (SDS) were purchased from Sigma Aldrich (Singapore). Various graphene nanoplatelets (graphene), as purchased from XG Science Inc., China, have specified average thicknesses of 1-2, 6-8, and 15 nm and platelet diameters of 2, 15, and 15 μm, in which they are referred to as graphene grade C (CG), graphene grade M (MG), and graphene grade H (HG), respectively.

6.3.2 Preparation of Graphene/Gelatin Hydrogel Composites

Various concentrations of graphene; 0.01, 0.1, 0.5, and 1 vol%, were dispersed in water solution filled with 1 vol% of SDS, sonicated via a transonicator

(Elma, S 70 H, D 78224) at room temperature, at 150 W, 50 Hz, for 15 min. Next, 10 vol% of gelatin was dissolved in distilled water (pH = 6.40) at 40 °C overnight via magnetic stirring. The two solutions were well–mixed at 40 °C, and poured into a petri dish to obtain the graphene/gelatin hydrogel composites. The hydrogel composites were allowed to set as a film at an ambient temperature (~ 30 °C). Each hydrogel composite had a thickness of ~1.59 mm.

6.3.3 Characterization and Testing of Graphene/Gelatin Hydrogel Composites

The true density of each graphene was measured by a gas pycnometer (Thermo Nicolet, Nexus 670) which was operated in He gas atmosphere (20 psi) at 25 °C with a purging gas time of 1 min. The true density of MWNT was measured repeatedly 20 times to obtain the average value and the standard deviation.

The Brunauer-Emmett-Teller (BET) surface area of graphene was measured through a Thermo Finnigan, Sorptomatic 1990 surface area analyzer (SAA). The samples were weighed and out-gassed at 300 °C for 12 h before measurement of the adsorption and desorption isotherms with He and N_2 gas.

Electrical conductivity of the graphene was measured at 25 °C. The fixture consisted of two probes, which made contact with the film surface. The fixture was connected to the power source (Keithley, Model 6517A) to supply a constant voltage source and read the current. The applied voltage and the resultant current were used to calculate electrical conductivity of the graphene samples by the following Eq. (6.1):

$$\sigma = \frac{I}{\rho} = \frac{I}{R_s t} = \frac{I}{KVt} \tag{6.1}$$

where σ is the specific conductivity (S/cm), ρ is the specific resistivity (Ω cm), t is the specimen thickness (cm), I is the measured resultant current (A), R_s is the sheet resistivity (Ω), V is the applied voltage (V), and K is the geometric correction factor.

The morphology and size of the graphene samples were observed using a H-7650 Transmission Electron Microscope (TEM; Hitachi High-Technology Corporation, Japan) at an operated voltage of 100 kV where imaging software (SEMAFORE 5.21) was used to determine platelet diameter of grapheme. Scanning electron micrographs of neat gelatin, and graphene/gelatin composites were obtained through a scanning electron microscope (SEM; S-4800, Hitachi, Japan) to determine the morphology at various graphene concentrations. The surface micrographs of neat gelatin and graphene/gelatin composites were taken using a voltage of 25 kV and a magnification of 10 000 times to observe the distribution of graphene in gelatin hydrogel composites.

Atomic force microscopy (AFM; Park system, XE-100) was used to observe the topology and phase images of the composites. Images were taken in the non–contact mode with the cantilever (NSC-14-CrAu) tapping at a scan rate of 0.25 Hz. The electrostatic force microscope (EFM) was utilized at a scan size of $1.00 \times 1.00\ \mu m^2$ using a signal amplitude of 5 V. Each sample was scanned at two heights above the surface. In the first level, the AFM topology images were obtained via scanning tip in the non–contact mode, which responded to the Van der Waals forces. The second scan measured the tip-surface distance as a result of the electrostatic force which was obtained from the charge distribution and the degree of charge generated in the gelatin and graphene/gelatin hydrogel composites.

A melt rheometer (Rheometric Scientific, ARES) was used to investigate the electromechanical properties of the gelatin and graphene/gelatin hydrogel composites. The samples were set with a parallel plate fixture at a diameter of 30 mm. DC voltage was applied at the electric field strength (800 V/mm) using a DC power supply (Instek, GFG8216A). First, a strain sweep test was operated to define the suitable strain for obtaining storage modulus (G') in the linear viscoelastic regime. The appropriate strain was determined to be 0.10 %strain for both of the gelatin hydrogel and the graphene/gelatin hydrogel composites. Second, the temporal response and the frequency sweep test were pre–sheared at a low frequency of 0.039811 rad/s and low strain of 0.10 % with the application of electric field (800 V/mm) for 15 min to assure with the equilibrium polarization in materials. In the frequency sweep test, the composite properties were measured as functions of

electric field strength (0–800 V/mm) and temperature (30–80 °C). The deflection of the gelatin hydrogel and the graphene/gelatin hydrogel composites was determined under the influence of applied electric strengths in the range of 0–600 V/mm). For each hydrogel composite, the sample was fixed vertically in a transparent chamber containing polydimethylsiloxane (PDMS) with the viscosity of 100 cSt between the copper electrodes as shown in Fig. 6.1. A high voltage power supply (Gamma High Voltage, UC5-30P) was connected to a DC power supply (Gold Sun 3000, GPS 3003D) for supplying DC electric field. The displacement of samples was recorded by using a digital video recorder (Sony, Handicam HR1). The composite deflection was measured with a Scion image (Beta 4.0.3) program.

The dielectrophoresis force is the deflecting force (F_d) generated which corresponds to the interaction between a non–uniform electric field and the resultant dipole moments of the material and was calculated with Eq. (6.2)

$$F_d = F_e + mg(\sin\theta) - \rho Vg(\sin\theta) \tag{6.2}$$

where F_e is the resisting elastic force (N), m is the mass of sample (kg), g is the gravity constant (9.8 m/s^2), θ is the deflection angle, ρ is the density of fluid, and V is the volume of the displaced fluid. In our experiment, the elastic force can be calculated by the following Eq. (6.3) (Sato *et al.*, 1996; Timoshenko *et al.*, 1970):

$$F_e = \frac{dEI}{l^3} \tag{6.3}$$

where E is the young's modulus which is equal to $2G'(1+\nu)$ in which G' is the shear modulus (taken to be G' (ω = 1 rad/s)) and ν is the Poisson's ratio, which is equal to 1/2 for an incompressible sample, I is the moment of inertia $t^3w/12$, t is the thickness of specimen, w is the width of specimen, d is the deflection distance, and l is the length of specimen

6.4 Result and Discussion

6.4.1 Characterization of Graphene

Characteristics of the different graphene samples are summarized in Table 6.1. The true densities of the three graphenes (grade C; CG, grade M; MG, and grade H; HG), as obtained from gas pycnometer, are 2.140 ± 0.10, 2.253 ± 0.12, and 2.202 ± 0.13 g/cm^3, respectively. In agreement, Nieto *et al.* (2012) found the similar density value of the graphene nanoplatelet to be 2.11 g/cm^3.

The surface area of MG exhibited the highest value of 389 m^2/g because its morphology consists of short stacks of graphene sheets. In general, the surface area of the graphene particles increases with decreasing particle size (Shirazi *et al.*, 2008). However, the measured surface area of CG was of the lowest value, since the CG particles form aggregates of platelets.

The morphologies and average diameters of the graphenes with various surface areas, measured by TEM, as shown in Fig. 6.2, are 1.098 ± 0.22, 12 ± 2.50, and 16 ± 2.13, consistent with the supplier material specifications.

The electrical conductivity values of CG, MG, and HG with different surface areas are approximately 3065 ± 38, 15 363 ± 393, and 8701 ± 80 S/cm as shown in Table 6.1. Thus, the highest electrical conductivity belongs to MG which also exhibits the highest surface area that shown in table1. The explanation for the electrical conductivity is that the greater surface area of the particles promotes electron transport well along the graphitic domain (Singh *et al.*, 2011; Paradee and Sirivat, 2014). Kuilla *et al.* (2010) reported the electrical conductivity of graphene to be as high as 7200 S/cm

6.4.2 Morphology, Topology, and Charge Distribution of Gelatin Hydrogel and Graphene/Gelatin Hydrogel Composites

Surface morphologies, appearing in SEM, of the gelatin and graphene/gelatin hydrogel composites are shown in Fig. 6.3a–c for the 0.1 vol% and 1 vol% MG which possesses the greatest surface area, electrical conductivity, and hydrophobic attraction force. It can be seen that the MG is well dispersed in the gelatin hydrogel at a low graphene concentration of 0.1 vol% with SDS as the

dispersing agent because the attractive hydrophobic force between graphene sheets is screened by the SDS molecules surrounding the graphene surface (Richard *et al.*, 2003). The distribution becomes relatively poorer at high MG (1 vol%) concentration, as shown in Fig. 6.3c, since the large hydrophobic interaction between the graphene molecules becomes more dominant and hampers uniform and homogeneous dispersion of 1 vol% MG in gelatin solution.

The topology and charge distribution on the surface of the MG/gelatin hydrogel composites can be observed by EFM at an external electric field of 5 V, as shown in Fig. 6.4. Figures 6.4a–c exhibit the topology of the gelatin hydrogel and the 0.1 vol% and 1 vol% MG/gelatin hydrogel composites without electrical field. Figure 6.4a shows the smooth surface of the pure gelatin hydrogel at nanoscale. A well-distributed and randomly-aligned of 0.1 vol% graphene in the gelatin hydrogel is confirmed through the topology image shown in Fig. 6.4b. On the contrary, Fig. 6.4c shows an agglomerated graphene (1 vol%) topology. Figures 6.4a′–c′ show the charge distribution of the gelatin hydrogel and the MG/gelatin hydrogel composites. The images appear as a bright contrast indicating the presence of the generated attractive force between the probe and the sample surface. The degree of generated attractive force on the gelatin hydrogel and the MG/gelatin hydrogel composites are shown in Fig. 6.5. Both 0.1 vol% and 1 vol% MG/gelatin hydrogel composites possess the degree of generated attractive force of 110 and 103 %, respectively, values which are greater than the pure gelatin hydrogel.

6.4.3 Electromechanical Properties

6.4.3.1 Time Dependence of the Electrorheological Response

First, the temporal responses of the pure gelatin and the graphene/gelatin hydrogel composites by alternately switched on and off were investigated under the applied electric field strength of E = 800 V/mm. The temporal characteristics of each material were determined under the linear viscoelastic regime under strain of 0.10 %, and frequency of 100 rad/s, where the time required for G' to respond is important in the actuator application. Induction time (τ_{ind}) is the time

required for G' to reach the steady state when E is switched on. Recovery time (τ_{rec}) is the time required for G' to decay toward its steady state, E is switched off.

From the previous works, Kunchornsup *et al.* (2012), Kunauraksapong *et al.* (2007), and Intanoo *et al.* (2012) investigated the τ_{ind} and τ_{rec} of cellulose gel, acrylic elastomer, and ethylene propylene diene elastomer (EPDM), in which the τ_{ind} and τ_{rec} of these materials were 130 s and 223 s, 418 s and 256 s, and 3735 s and n/a s, respectively. The τ_{ind} and τ_{rec} of 0.1 vol% graphene/gelatin hydrogel composite provided the lowest τ_{ind} and τ_{rec} among other materials at 103 s and 171 s, respectively. Figure 6.6 shows the comparison of G' of the pure gelatin and the graphene/gelatin hydrogel composites (0.1 vol% and 1 vol%) during the time sweep test under the influence of an electric field. For the pure gelatin hydrogel, G' rapidly reaches a steady-state value as the electric field is applied. This is due to the induced dipole moment generated within the gelatin molecules. The G' decreases immediately and recovers closely its original value as electric field is switched off, suggesting it is nearly a reversible material. On the other hand, for both graphene/gelatin hydrogel composites (0.1 vol% and 1 vol%), The G' does not recover to its original value as electric field is switched off. Possibly, there are some residue dipole moments remaining in the agglomeration of the graphene particles (Tungkavet *et al.*, 2011).

6.4.3.2 *Effects of Electric Field Strength and Surface Area on Electromechanical Properties of Graphene/Gelatin Hydrogel Composites*

The graphene hydrogel composite, 0.1 vol%, was investigated further for the electromechanical properties under the effect of graphene surface areas of 41, 115, and 388 m^2/g for the CG, HG, and MG graphenes, respectively, at an electric field range of 0–800 V/mm. The storage modulus response ($\Delta G'$) and the storage modulus sensitivity ($\Delta G'/G'_o$) of the composites are shown in Fig. 6.7 at a frequency of 100 rad/s, a strain of 0.10 %, and at a temperature of 30 °C. The $\Delta G'$ and $\Delta G'/G'_o$ of 0.1 vol% graphene/gelatin hydrogel composites increase with increasing electric field strength and with increased graphene surface

area due to the generated polarization on carboxyl groups within the gelatin molecule leading to intermolecular interactions (Tungkavet *et al.*, 2011). It should be noted that there are two reasons for the higher response of gelatin hydrogel composites with greater graphene surface area: a stronger interfacial force between the nano-particle and the matrix due to a higher surface area (Ayatollahi *et al.*, 2011); or the nanoparticle-matrix interaction, leading to a stronger intermolecular interaction (Boo *et al.*, 2007) Thus, the embedded nano-particles can enhance G′ of the gelatin hydrogel.

Rafiee *et al.* (2009) investigated improved mechanical properties of nanocomposites with a low graphene concentration at a weight fraction of 0.1 %. The 0.1 wt% graphene/epoxy nanocomposite possessed superior mechanical properties relative to CNT nanocomposites, namely the Young's modulus, tensile strength, and toughness since the enhanced surface area of graphene induced higher nanoparticle-matrix interaction.

6.4.3.3 Effect of Concentration on Electromechanical Properties of Graphene/Gelatin Hydrogel Composites

The effect of graphene concentration on the electromechanical properties of the graphene/gelatin hydrogel composites was investigated under an applied electric field strength of 0–800 V/mm. The $\Delta G'$ of the composites vs electric field strength are shown in Fig. 6.8. The $\Delta G'$ increases nonlinearly with increasing electric field strength (0–800 V/mm). The $\Delta G'$ at an applied electric field strength of 800 V/mm reaches values as high as 78 000, 456 000, 1 254 000, 283 000, and 128 000 at graphene concentrations of 0, 0.01, 0.1, 0.5, and 1 vol%, respectively. The $\Delta G'/G'_o$ values of the graphene/gelatin hydrogel composites are also tabulated in Table 6.2. The increase of graphene concentration leads to the increase of G'_o since the nanoplatelets act as a reinforcement filler (Tungkavet *et al.*, 2012). Furthermore, under electric field the induced dipole moments from the enhanced polarized carboxyl groups of gelatin molecule are generated and interact with the embedded graphene. Table 6.3 shows the storage modulus sensitivity characteristics of several electroactive polymers and dielectric elastomers. The $\Delta G'/G'_o$ comparison of these materials can be made between Tables

6.2 and 6.3. The polyesterurethane (LPR) exhibits the highest sensitivity under the dielectric elastomer type, in which the $\Delta G'/G'_o$ is 2.08 at 2000 V/mm. In our work, the 0.1 vol% graphene/gelatin hydrogel composite storage modulus sensitivity is 3.52 of E = 800 V/mm, clearly a superior response relative other materials. The maximum $\Delta G'$ and $\Delta G'/G'_o$ values obtained belong to the 0.1 vol% graphene/gelatin hydrogel composite. Furthermore, both $\Delta G'$ and $\Delta G'/G'_o$ decreased with graphene concentration greater than 0.1 vol%. The poorly dispersed graphene leads to the phase separation between the gelatin hydrogel and the graphene agglomeration, as previously observed in the SEM and topology surface images in Figs. 6.3c and 6.4c. Although $\Delta G'/G'_o$ values of 0.5 and 1 vol% graphene composites are reduced relative to the 0.01 and 0.1 vol% graphene, they still were greater than that of the pure gelatin hydrogel, dielectric elastomers, and other electroactive materials.

Rashad *et al.* (2014) studied the effect of graphene distributed in an aluminum matrix. 0.3 wt% of embedded graphene in Al was dispersed homogeneously, acting as a reinforcement filler to enhance yield strength and ultimate tensile strength.

Wan *et al.* (2011) reported that the Young's moduli of graphene oxide/gelatin nanocomposites increased with an addition of 1 wt% GO due to the size, morphology, and dispersion degree of the GO nanosheet in the gelatin material.

Shen *et al.* (2013) reported the similar result of the tensile strength in the graphene/epoxy nanocomposites at graphene concentrations between 0.25 to 1.50 wt%. The strength of the nanocompsites decreased as the graphene concentration increased to 0.5, 1, and 1.5 wt% because the aggregation of graphene occurred in the matrix, resulting in steric hindrance.

Liu and Shaw (2001) found that the modulus of the blended silica in silicone rubber decreased with silica content above 55 vol% due to the steric hindrance effect.

6.4.3.4 Effect of Operating Temperature

The effect of temperature on the pure gelatin and the graphene/gelatin hydrogel composites are shown in Fig. 6.9, at the frequency of 100

rad/s and 800 V/mm. Figure 6.9 compares $G'_{800v/mm}$ and $\Delta G'$ vs. temperature of the pure gelatin hydrogel and 0.1 vol% graphene/gelatin hydrogel composite which consists of three phases. In the first phase, $G'_{800v/mm}$ and $\Delta G'$ decrease with increasing temperature from 30 °C to 40 °C due to the conformational change from the denatured helix gelatin to random coil molecules (Bigi *et al.*, 2004). In the second phase, at the temperature range of 40–50 °C, $G'_{800v/mm}$ and $\Delta G'$ of the composites increase, which is consistent with the classical network theory (Sato *et al.*, 1996). The higher temperature introduces more entropy into the systems, leading to greater retractive force and induced physical entanglement. However, the decrease in $G'_{800v/mm}$ of the pure gelatin and the composite occurs in the third phase with temperatures above 60 °C since α-amino acid block of the gelatin chain is isolated at a temperature close to the low-temperature glass transition of 120 °C (Fraga *et al.*, 1985). Obviously, $G'_{800v/mm}$ and $\Delta G'$ of the composites are greter than those of the pure gelatin hydrogel at any temperatures due to the enhanced polarizability of the carboxyl groups within the gelatin chains. In summary, the electomechanical properties of the graphene/gelatin hydrogel composites are greatly enhanced via the graphene addition.

6.4.4 Deflection of Graphene/Gelatin Hydrogel Compsites

The deflection response (d) and dielectrophoresis forces (F_d) of the pure gelatin and hydrogel composites were investigated under an electric field strength of 600 V/mm. The samples were attached between two copper electrodes (one anode and another neutral) in a PDMS chamber as shown in Fig.6.1. Under the influence of electric field strength, the samples deflected toward the anode side as shown in Figs. 6.10a–c, indicating the attractive force that was generated from the polarized carbonyl groups in the gelatin molecule to the anode side; the polarized carboxyl groups produced the net negative charges in the gelatin structure. The pure gelatin, 0.1 vol%, and 1 vol% graphene/gelatin hydrogel started to deflect at the critical electric field strengths of 100 V/mm, 50 V/mm, and 150 V/mm, respectively. The 0.1 vol% graphene/gelatin hydrogel composite also exhibited the largest deflection distance than pure gelatin and 1 vol% graphene/gelatin hydrogel composite at 600 V/mm because the greater amount of polarization was generated

through the graphene. Conversely, the 1 vol% graphene/gelatin hydrogel composite exibited the lowest deflection distance among others as excessively high amount of graphene nanosheet obstructed the polarization (Krause *et al.*, 2001).

Niamlang *et al.* (2008) showed the similar results of deflection of poly(p-phenylenevinylene)/polydimethylsiloxane blends (PPV/PDMS). The maximum dielectrophoresis force was found in PPV/PDMS-10 due to greater amounts of polarized particles: however, the PPV/PDMS-20 showed a lower dielectrophoresis force than PPV/PDMS-10 due to too high particle concentration and particle steric hindrance.

Hiamtup *et al.* (2008) reported the bending distance of polyaniline blended in poly (dimethyl siloxane) (PANI/PDMS). The deflection of 20 vol% PANI/PDMS was less than 10 vol% PANI/PDMS since the higher particle amount screened the particle-matrix interaction and decreased the polarizability in the blended material.

The d and F_d of the pure gelatin and the graphene/gelatin hydrogel composites with applied electric field strength are exhibited in Figs. 6.11a–b. Under higher applied electric field, larger dipole moments are created, inducing greater d and F_d from these materials. The d of the pure gelatin, 0.1 vol%, and 1.0 vol% graphene/gelatin hydrogel composites are 13.5, 14.7, and 13.1 mm, and F_d of the pure gelatin, 0.1 vol%, and 1.0 vol% graphene/gelatin hydrogel composites are 0.032, 0.082, and 0.029 N, respectively. It was found that the 0.1 vol% MWNT/gelatin hydrogel composite show the highest d and F_d values due to the highest amount of polarized carboxyl groups through the suitable graphene content, mentioned in the result of the degree of generated attractive force in Fig.6.5.

Petcharoen *et al.* (2013) reported the d and F_d of Poly(ester-urethane) (LPR). At E = 550 V/mm, LPR achieved the greatest d and F_d at 10 mm and 43μN, respectively.

Thongsak *et al.* (2010) reported that the maximum d and the F_d of styrene-isoprene-styrene triblock copolymer (SIS) to be 2.86 mm and 36.4 μN, respectively at applied electric field strength of 600 V/mm.

Tungkavet *et al.* (2012) investigated the F_d of nanowire polypyrrole/gelatin hydrogel under electric field strength of 600 V/mm. Nanowire

Ppy/gelatin composites (0.1 vol%) achieved a higher F_d (6.60 mN) than 1 vol% nanowire Ppy added because the chemical structure of PPy possessed the positive charges from the amine groups, leading to interference on the negative charges of the gelatin molecules.

The 0.1 vol% graphene/gelatin hydrogel composite in the current study provides the largest d and F_d at 14.7 mm and 0.082 N, the latter is much higher than materials in other studies.

6.5 Conclusions

In our study, the electromechanical properties of the pure gelatin and graphene/gelatin hydrogel composites were investigated under applied electric field strength under the effects of surface area, graphene concentration, and temperature. The highest surface area of graphene blended in gelatin provided the highest storage modulus response ($\Delta G'$) and storage modulus sensitivity ($\Delta G'/G_o$) due to the strongest interfacial force between the nano-particles and the matrix, leading to the enhanced polarization on the carboxyl groups in the gelatin molecules with the presence of graphenes. The $\Delta G'$ increased significantly with increasing graphene concentration from 0 to 0.1 vol% under applied electric field strengths of 0–800 V/mm. The maximum $\Delta G'$ and $\Delta G'/G_o$ were 1.25×10^6 Pa and 3.52, respectively, for the 0.1 vol% graphene/gelatin hydrogel composite. For the influence of temperature, both G' and $\Delta G'$ showed three regime behaviors in the temperature range of 30–90 °C. Lastly, the deflection distance (d) and the dielectrophoresis force (F_d) of the pure gelatin, 0.1 vol%, and 1 vol% graphene/gelatin hydrogel composites increased monotonically with increasing electric field strength. The 0.1 vol% graphene/gelatin hydrogel composite delivered the greatest d and F_d suggesting that it is the most suitable candidate for actuator applications.

6.6 Acknowledgements

The authors appreciate the financial supports provided by the Conductive and Electroactive Polymers Research Unit (CEAP) of Chulalongkorn University; the Thailand Research Fund (TRF); the Royal Thai Government; the 90th Anniversary of Chulalongkorn University Fund (Ratchadaphiseksomphot Endowment Fund); the Petroleum and Petrochemical College (PPC), Chulalongkorn University; and the Doctoral Scholarship from the Thailand Graduate Institute of Science and Technology (TGIST) (TG-33-09-53-003D).

6.7 References

Ayatollahi, M.R., Shadlou, S., Shokrieh, M.M., and Chitsazzadeh, M. (2011) Effect of multi-walled carbon nanotube aspect ratio on mechanical and electrical properties of epoxy-based nanocomposites. Polymer Testing, 30, 548–556.

Bae, Y.H., Okano, T., Hsu, R., and Kim, S.W. (1987) Thermo-sensitive polymers as on-off switches for drug release. Macromolecular Rapid Communications, 8, 481-485.

Balandin, A.A., Ghosh, S., Bao, W., Calizo, I., Teweldebrhan, D., and Miao, F. (2008) Superior thermal conductivity of single-layer graphene. Nano Letters, 28, 902-907.

Bar-Cohen, Y. (2004) Electroactive Polymer (EAP) as Artificial Muscles: Reality, Potential, and Challenges, 2nd ed. Bellingham, Washington: SPIE Press.

Bigi, A., Panzavolta, S., and Rubini, K. (2004) Relationship between triple-helix content and mechanical properties of gelatin films. Biomaterials, 25, 5675-5680.

Boo, W.J., Sun, L., Warren, G.L., Moghbelli, E., Pham, H., Clearfield, A., and Sue, H.J. (2007) Effect of nanoplatelet aspect ratio on mechanical properties of epoxy nanocomposites. Polymer, 48, 1075–1082.

Fraga, A.N. and Williams, R.J.J. (1985) Thermal properties of gelatin films. Polymer, 26, 113-118.

Goenka, S., Sant, V., and Sant, S. (2014) Graphene-based nanomaterials for drug delivery and tissue engineering. Journal of Controlled Release, 173, 75-88.

Hiamtup, P., Sirivat, A., and Jamieson, A.M. (2008) Electromechanical response of a soft and flexible actuator based on polyaniline particles embedded in a cross-linked poly(dimethyl siloxane) network. Materials Science and Engineering: A, 28, 1044-1051.

Hoffman, S.A. (1987) Applications of thermally reversible polymers and hydrogels in therapeutics and diagnostics. Journal of Controlled Release, 6, 297-305.

Ionita, M., Pandele, M.A., and Iovu, H. (2013) Sodium alginate/graphene oxide composite films with enhanced thermal and mechanical properties. Carbohydrate Polymers, 94, 339-344.

Intanoo, P., Sirivat, A., Kunanuruksapong, R., Lerdwijitjarud, W., and Kunchornsup,W. (2012) Electroactive polymer actuator from highly doped permethylpolyazine dispersed in ethylene propylene diene elastomer. Journal of Polymer Research, Doi 10.1007/s10965-012-9981-7.

Kim, H.S., Li, Y., and Kim, J. (2008) Electro-mechanical behavior and direct piezoelectricity of cellulose electro-active paper. Sensors and Actuators A: Physical, 147, 304-309.

Kim, S.J., Lee, K.J., Kim, S.I., Lee, Y.M., Chung, T.D., and Lee, S.H. (2002) Electrochemical behavior of an interpenetrating polymer network hydrogel composed of poly(propylene glycol) and poly(acrylic acid). Journal of Applied Polymer Science, 89, 2301–2305.

Kim, S.J., Park, S.J., Kim, I.Y., Shin, M.S., and Kim, S.I. (2002) Electric stimuli response to poly(vinyl alcohol)/chitosan interpenetrating polymer network hydrogel in NaCl solutions. Journal of Applied Polymer Science, 86, 2285-2289.

Krause, S. and Bohon, K. (2001) Electromechanical response of electrorheological fluids and poly(dimethylsiloxane) networks. Macromolecule, 34, 7179–89.

Kuilla, T., Bhadra, S., Yao, D., Kim, N.H., Bose, S., and Lee, J.H. Recent advances in graphene based polymer composites. Progress in Polymer Science, 35, 1350-1375.

Kujawski, M., Pearse, J.D., and Smela, E. (2010) Elastomers filled with exfoliated graphite as compliant electrode. Carbon, 48, 2409-2417.

Kunchornsup, W. and Sirivat, A. (2012) Physically cross-linked cellulosic gel via 1-butyl-3methylimidazolium chloride ionic liquid and its electromechanical responses. Sensors and Actuators A: Physical, 175, 155-164.

Kunanuruksapong, R. and Sirivat, A. (2008) Electrical properties and electromechanical responses of acrylic elastomers and styrene copolymers: effect of temperature. Applied Physics A, 92, 313-320.

Kwon, I.C., Bae, Y.H., and Kim, S.W. (1991) Electrically erodible polymer gel for controlled release of drugs. Nature, 354, 291-293.

Lee, C., Wei, X., Kysar, J.W., and Hone, J. (2008) Measurement of the elastic properties and intrinsic strength of monolayer graphene. Science, 321, 385-388.

Liang, J., Huang, Y., Zhang, L., Wang, Y., Ma, Y., Guo, T., and Chen, Y. (2009) Molecular-level dispersion of graphene into poly (vinyl alcohol) and effective reinforcement of their nanocomposites. Advanced Functional Materials, 19, 1-6.

Liu, B. and Shaw, T.M. (2001) Electrorheology of filled silicone elastomers. Journal of Rheology, 45, 641-657.

Miyata, T., Asami, N., and Uragami, T. (1999) A reversibly antigen-responsive hydrogel. Nature, 399, 766-769.

Niamlang, S. and Sirivat, A. (2008) Dielectrophoresis force and deflection of electroactive poly(p-phenylene vinylene)/polydimethylsiloxane blends. Smart Materials and Structure, 17, 1–8.

Nieto, A., Lahiri, D., and Agarwal, A. (2012) Synthesis and properties of bulk graphene nanoplatelets consolidated by spark plasma sintering. Carbon, 50, 4068-4077.

Novoselov, K.S., Geim, A.K., Morozov, S.V., Jiang, D., Zhang, Y., and Dubonos, S.V. (2004) Electric field effect in atomically thin carbon films. Science, 306, 666–669.

Okano, T., Bae, Y.H., Jacobs, H., and Kim, S.W. (1990) Thermally on-off switching polymers for drug permeation and release. Journal of Controlled Release, 11, 255-265.

Paradee, N. and Sirivat, A. (2014) Synthesis of poly(3,4-ethylenedioxythiophene) nanoparticles via chemical oxidation polymerization. Polymer Internaional, 63, 106-113.

Petcharoen, K. and Sirivat, A. (2013) Electrostrictive properties of thermalplastic polyurethane elastomer: Effects of urethane type and soft–hard segment composition. Current Applied Physics, 13, 1119–1127.

Rafiee, M.A., Rafiee, J., Wang, Z., Song, H., Yu, Z.Z., and Koratkar, N. (2009) Enhanced mechanical properties of nanocomposites at low graphene content. American Chemical Society Nano, 3, 3884-3890.

Rashad, M., Pan, F., Tang, A., and Asif, M. (2014) Effect of graphene nanoplatelets addition on mechanical properties of pure aluminum using a semi-powder method. Progress in Natural Science: Materials International, 24, 101-108.

Richard, C., Balavoine, F., Schultz, P., Ebbesen, T.W., and Mioskowski, C. (2003) Supramolecular self-assembly of lipid derivatives on carbon nanotubes. Science, 300, 775–778.

Sato, T., Watanabe, H., and Osaki, K. (1996) Rheological and dielectric behavior of a styrene-isoprene-styrene triblock copolymer in n-tetradecane. 1. Rubbery-Plastic-Viscous transition. Macromolecule, 29, 6231-6239.

Shen, M.Y., Chang, T.Y., Hsieh, T.H., Li, Y.L., Chiang, C.L., Yang, H., and Yip, M.C. (2013) Mechanical properties and tensile fatigue of graphene nanoplatelets reinforced polymer nanocomposites. Journal of Nanomaterials, 2013, 1-9.

Shiga, T. (1997) Deformation and Viscoelastic Behavior of Polymer Gels in Electric Fields. Advances in Polymer Science. (pp. 134). Berlin: Springer-Verlag.

Shirazi, L., Jamshidi, E., and Ghasemi, M.R. (2008) The effect of Si/Al raio of Zsm-5 zeolite on its morphology, acidity, and crystal size. Crystral and Research Technology, 43, 1300-1306.

Siegel, R.A. and Firestone, B.A. (1988) pH-dependent equilibrium swelling properties of hydrophobic polyelectrilyte copolymer gels. Macromolecules, 21, 3254-3259.

Singh, V., Joung, D., Zhai, L., Das, S., Khondaker, S.I., and Seal, S. (2011) Graphene based materials: Past, present, and future. Progress in Materials Science, 56, 1178-1271.

Tanaka, T., Fillmore, D., Sun, S.T., Nishio, I., Swislow, G., and Shah, A. (1980) Phase transitions in ionic gels. Physical Review Letters, 45, 1636-1639.

Tanaka, T., Nishio, I., Sun, S.T., and Ueno-Nishio, S. (1982) Collapse of gels in an electric field. Science, 218:467-469.

Timoshenko, S.P. and Goodier, J.N. (1970) Theory of Elasticity. Auckland: McGraw-Hill.

Thongsak, K., Kunanuruksapong, R., Sirivat, A., and Lerdwijitjarud, W. (2010) Electroactive styrene-isoprene-styrene triblock copolymer: Effect of morphology and electric field. Materials Science and Engineering: A, 527, 2504–2509.

Tungkavet, T., Pattavarakorn, D., and Sirivat, A. (2012) Bio-compatible gelatins (Ala-Gly-Pro-Arg-Gly-Glu-4Hyp-Gly-Pro-) and electromechanical properties: effects of temperature and electric field. Journal of Polymer Research, 19, 9759-3.

Tungkavet, T., Seetapan, N., Pattavarakorn, D., and Sirivat, A. (2012) Improvements of electromechanical properties of gelatin hydrogels by blending with nanowire polypyrrole: Effects of electric field and temperature. Polymer International, 61, 825-833.

Wan, C., Frydrych, M., and Chen, B. (2011) Strong and bioactive gelatin/graphene oxide nanocomposites. Soft Matter, 7, 6159-6166.

Wang, W., Wang, Z., Liu, Y., Li, N., Wang, W., and Gao, J. (2012) Preparation of reduced graphene oxide/gelatin composition films with reinforced mechanical strength. Materials Research Bulletin, 47, 2245-2251.

Yang, X.J., Zheng, P.J., Cui, Z.D., Zhao, N.Q., Wang, Y.F., and Yao, K.D. (1997) Swelling behavior of elastic properties of gelatin gels. Polymer International, 44, 448-452.

Zareie, H.M., Bulmus, E.V., Gunning, A.P., Hoffman, A.S., Piskin, E., and Morris, V.J. (2000) Investigation of stimuli-responsive copolymer by atomic force microscopy. Polymer, 41, 6723–6727.

Zhang, L., Wang, Z., Xu, C., Li, Y., Gao, J., Wang, W., and Liu, Y. (2011) High strength graphene oxide/polyvinyl alcohol composite hydrogel. Journal of Materials Chemistry, 21, 10399-10406.

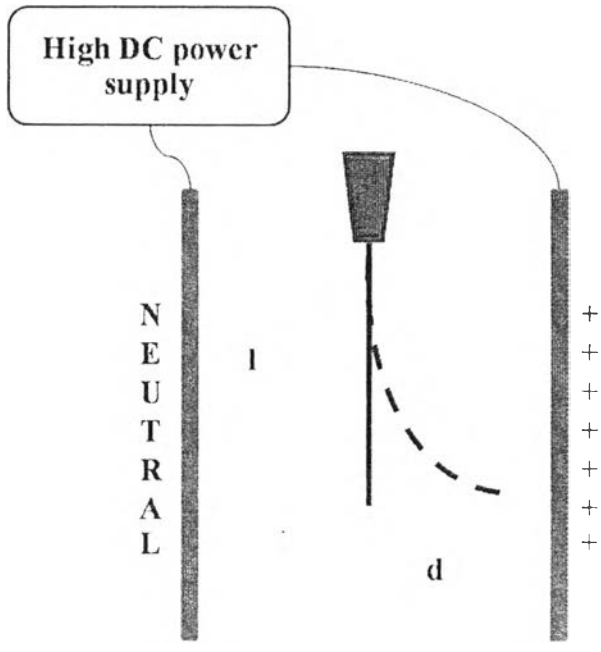

Figure 6.1 Schematic diagram of the apparatus used to observe the dielectrophoresis force on the hydrogel samples.

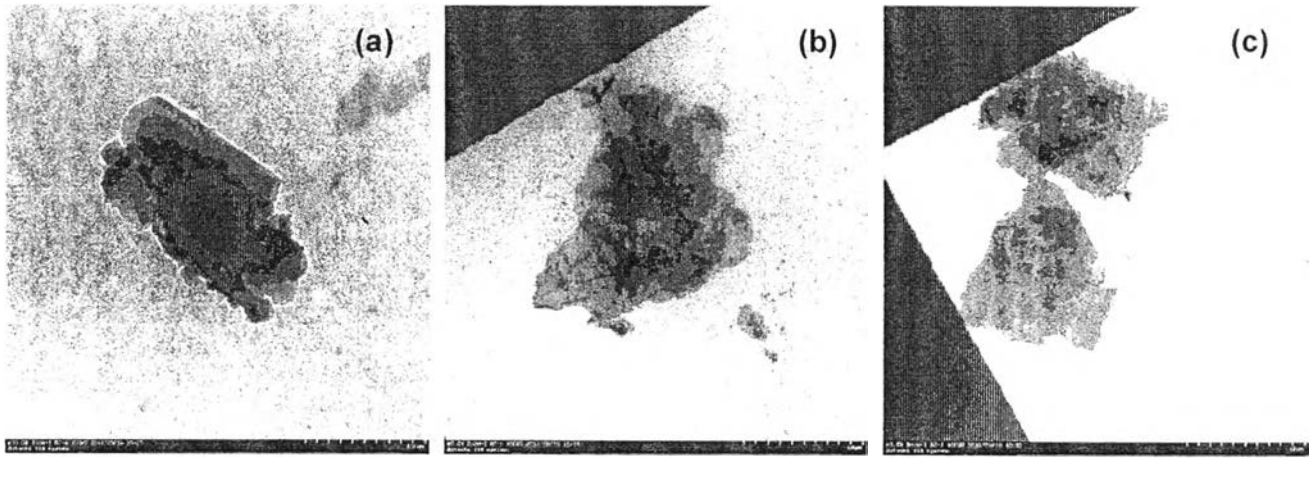

Figure 6.2 TEM micrographs of (a) graphene (CG) at magnification of 10K; (b) graphene (MG) at magnification of 0.5K; and (c) graphene (HG) at magnification of 0.5K.

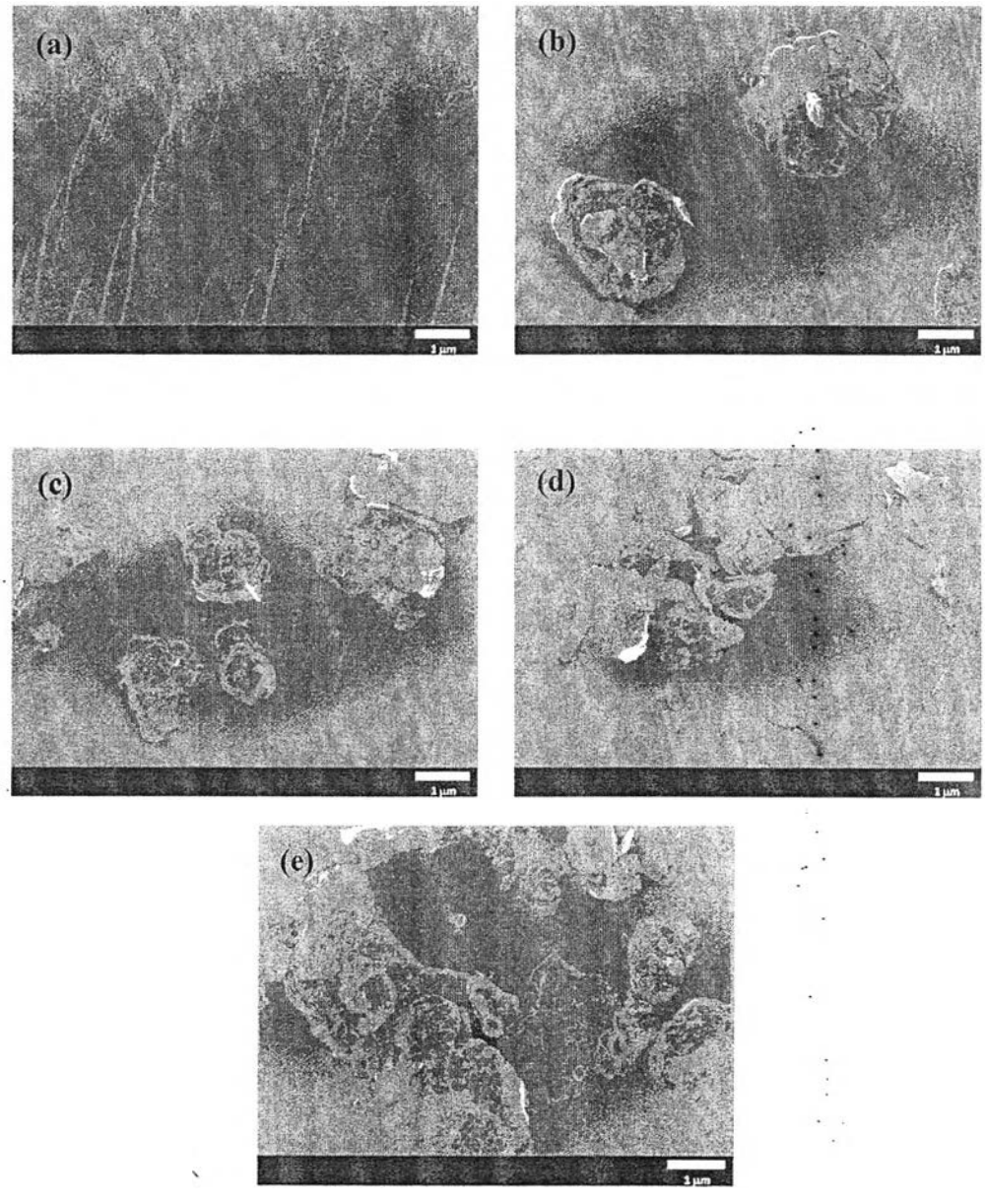

Figure 6.3 SEM micrographs of pure gelatin and graphene/gelatin composites at magnification of 10K: (a) pure gelatin; (b) 0.01 vol% graphene/gelatin composite; (c) 0.1 vol% graphene/gelatin composite; (d) 0.5 vol% graphene/gelatin composite; (e) 1 vol% graphene/gelatin composite.

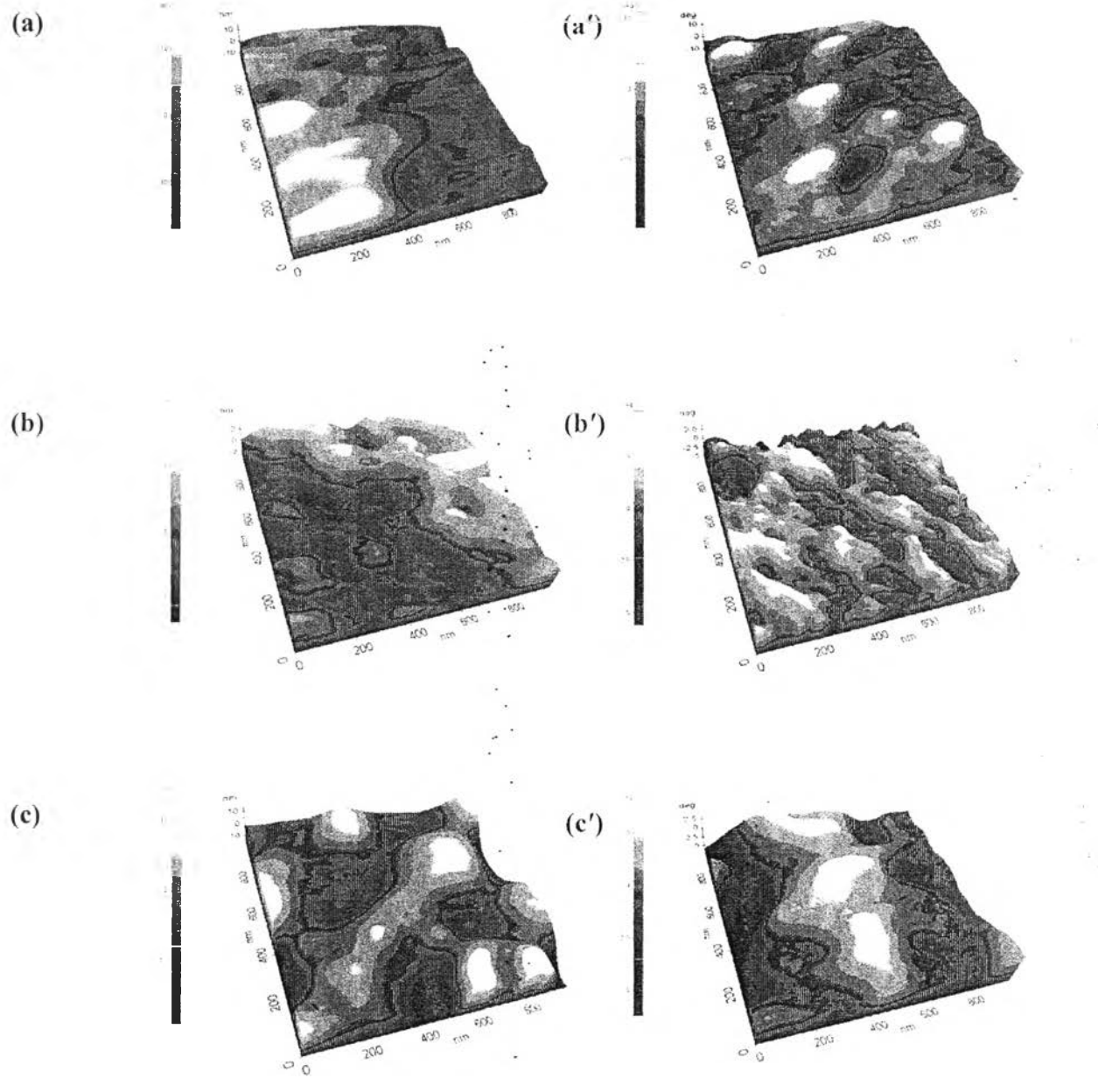

Figure 6.4 (a) Topology image of pure gelatin hydrogel; (a′) EFM image under 5V of sample voltage bias of pure gelatin hydrogel; (b) Topology image of 0.1 vol% graphene/gelatin hydrogel; (b′) EFM image under 5V of tip voltage bias of 0.1 vol% graphene/gelatin hydrogel; (c) Topology image of 1 vol% graphene/gelatin hydrogel; (c′) EFM image under 5V of tip voltage bias of 1 vol% graphene/gelatin hydrogel.

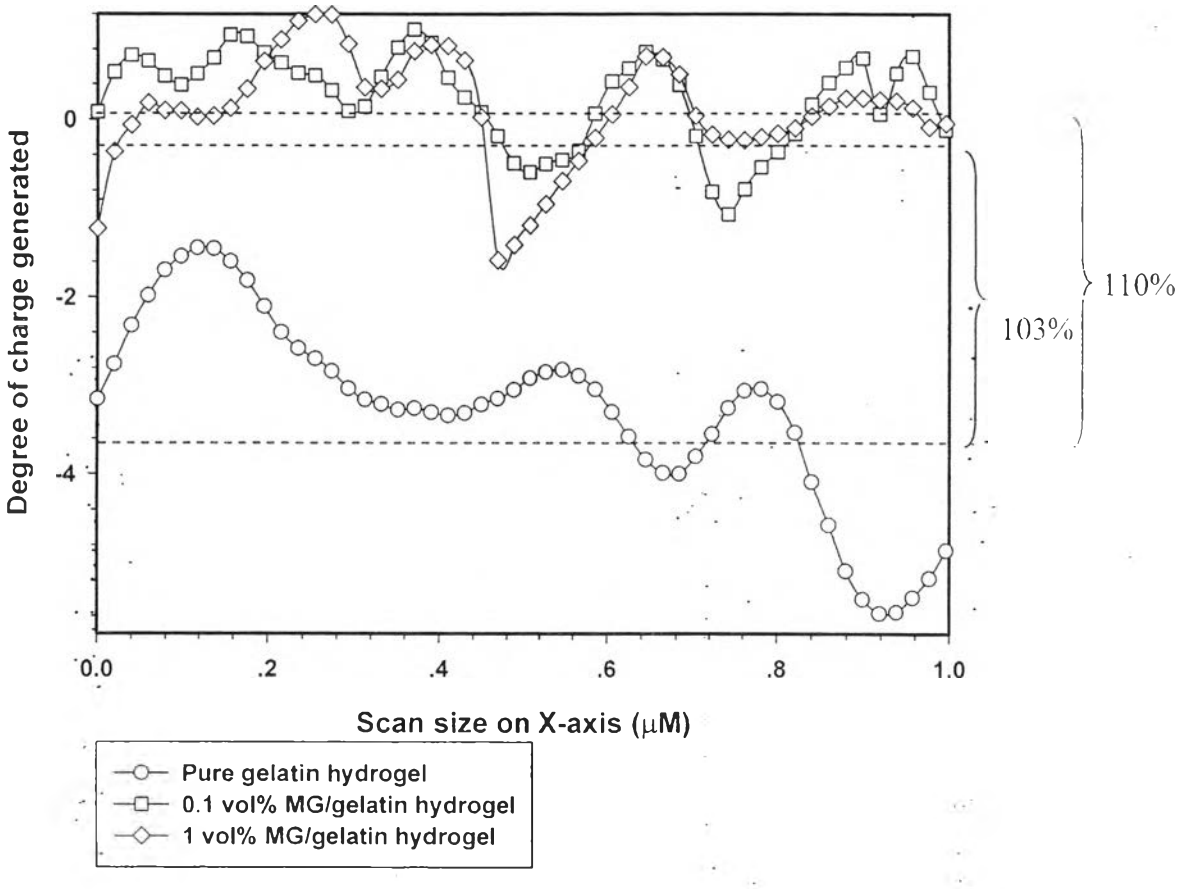

Figure 6.5 Degree of charge generated on graphene/gelatin hydrogel composites under 5 V of tip bias at whole region.

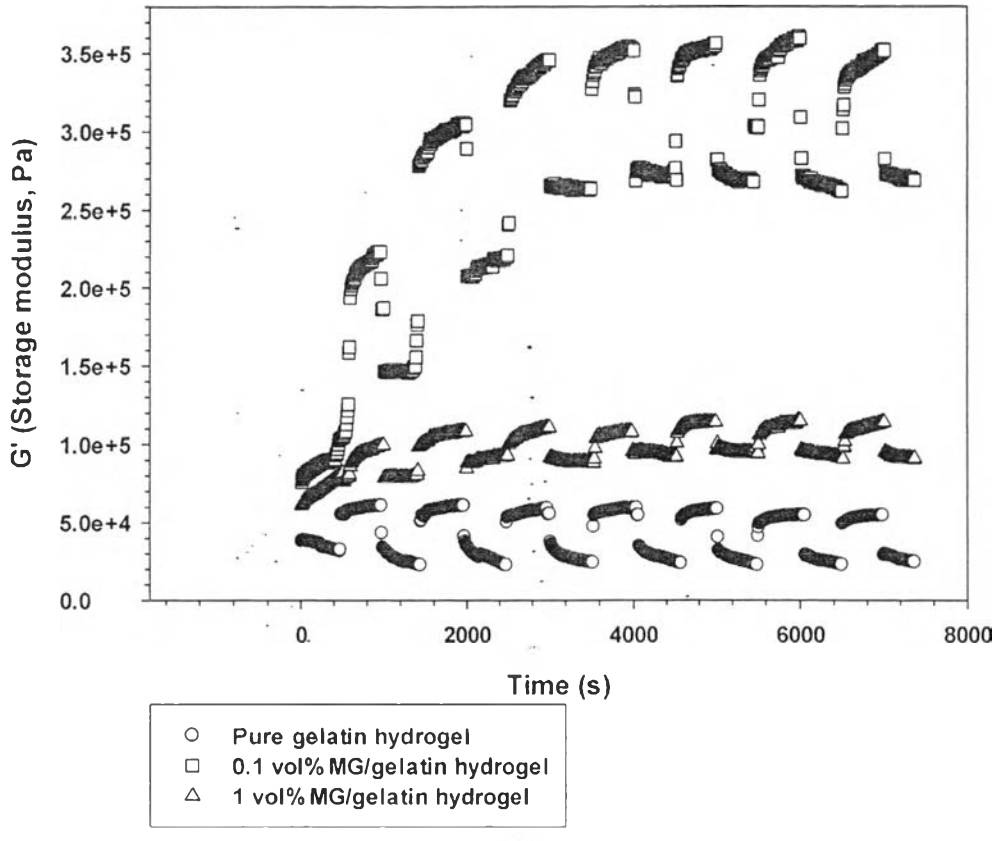

Figure 6.6 Temporal responses of the storage modulus (G') of the pure gelatin hydrogel and the graphene/gelatin hydrogels (sample diameter 30 mm, gel thickness 1.590 mm, 0.10 %strain, frequency of 100 rad/s, 800 V/mm, 30 °C): pure gelatin hydrogel (○); 0.1 vol% MG/gelatin hydrogel (□); and 1 vol% MG/gelatin hydrogel (△).

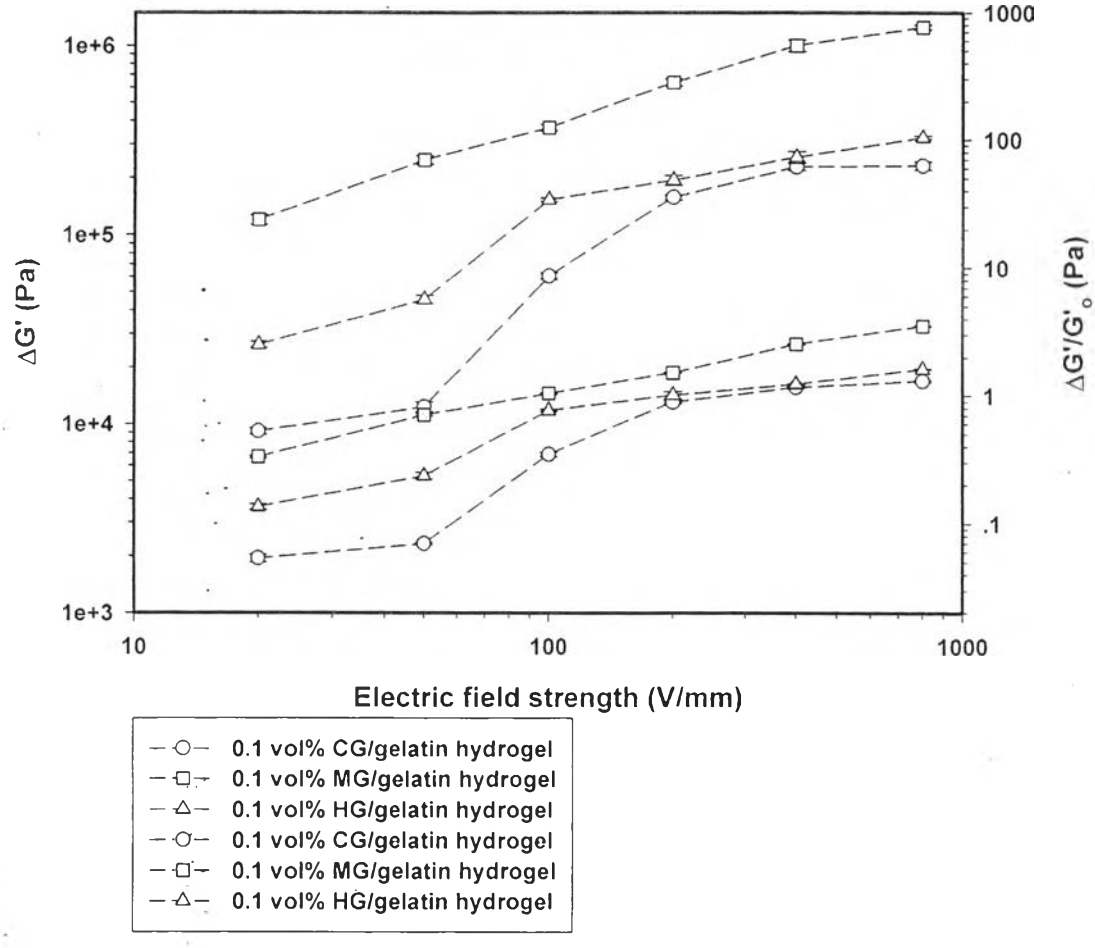

Figure 6.7 Effect of surface area of graphene on the storage modulus response ($\Delta G'$) and storage modulus sensitivity ($\Delta G'/G'_o$) at various electric field strengths (sample diameter 30 mm, gel thickness 1.590 mm, 0.10 %strain, frequency of 100 rad/s, 30 °C).

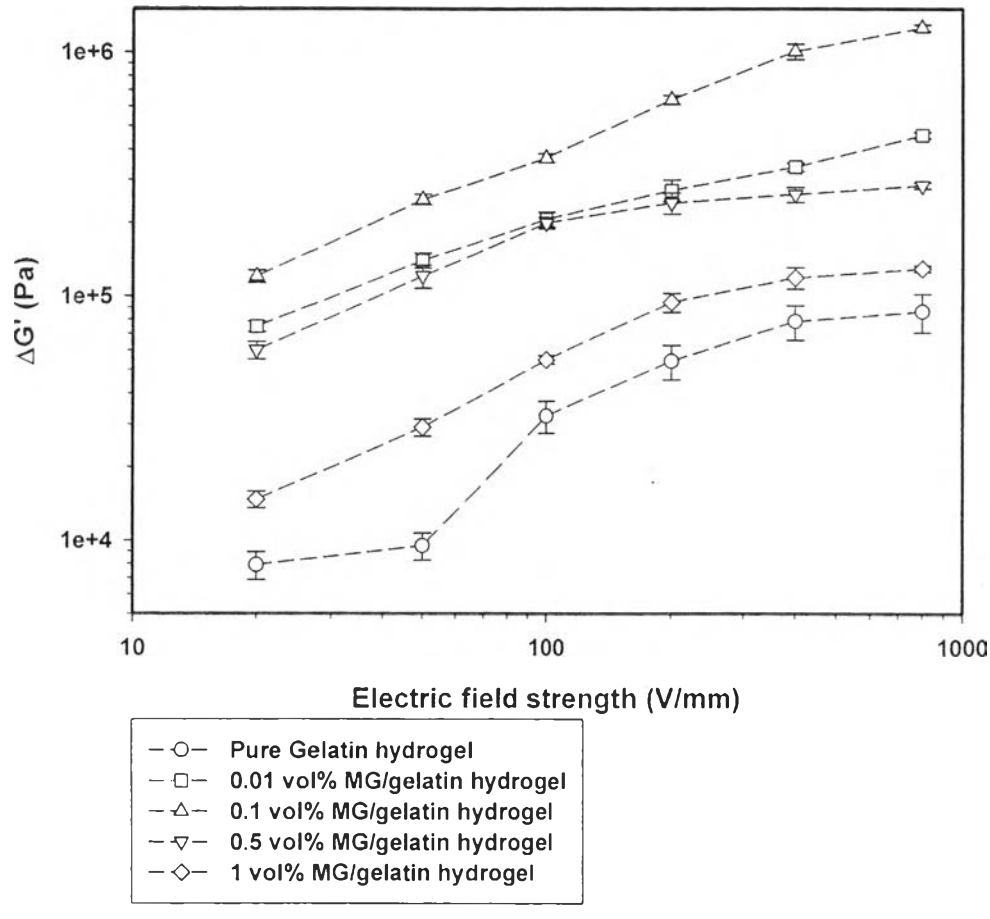

Figure 6.8 Effect of concentration of MG/gelatin hydrogel on the storage modulus response ($\Delta G'$) at various electric field strengths (sample diameter 30 mm, gel thickness 1.590 mm, 0.10 %strain, frequency of 100 rad/s, 30 °C).

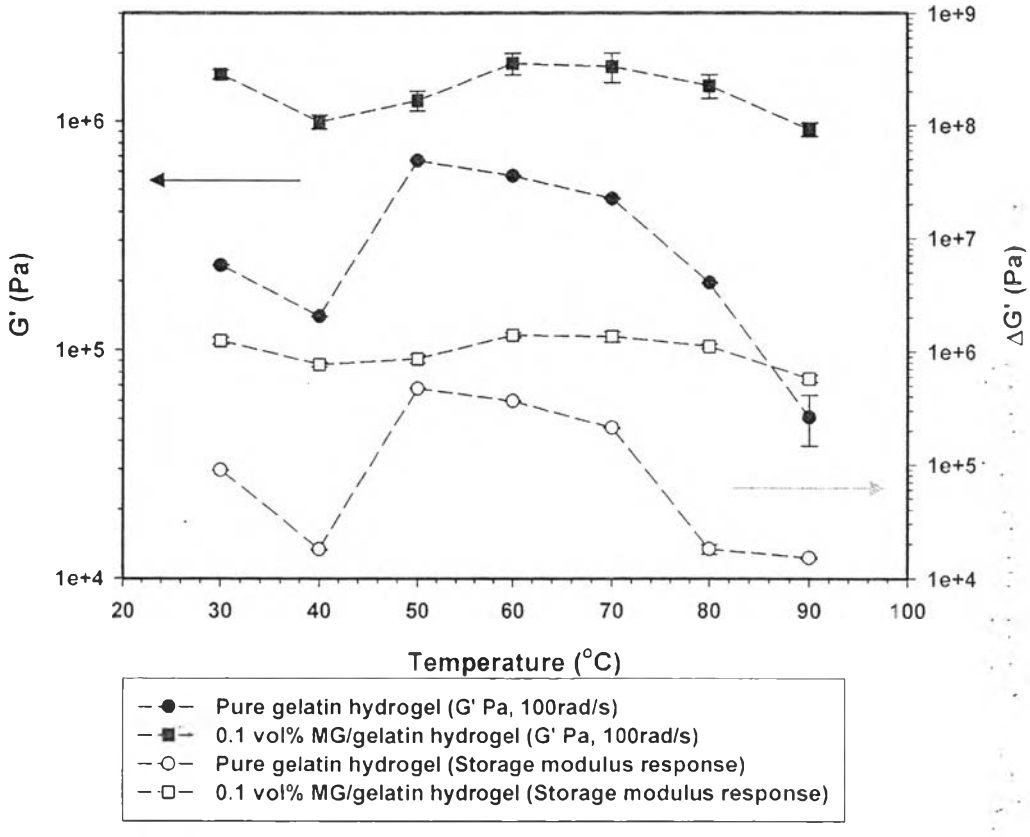

Figure 6.9 Effect of concentration of graphene on the storage modulus (G') and storage modulus response ($\Delta G'$) at various temperatures (sample diameter 30 mm, gel thickness 1.590 mm, 0.10 %strain, frequency of 100 rad/s, 800 V/mm).

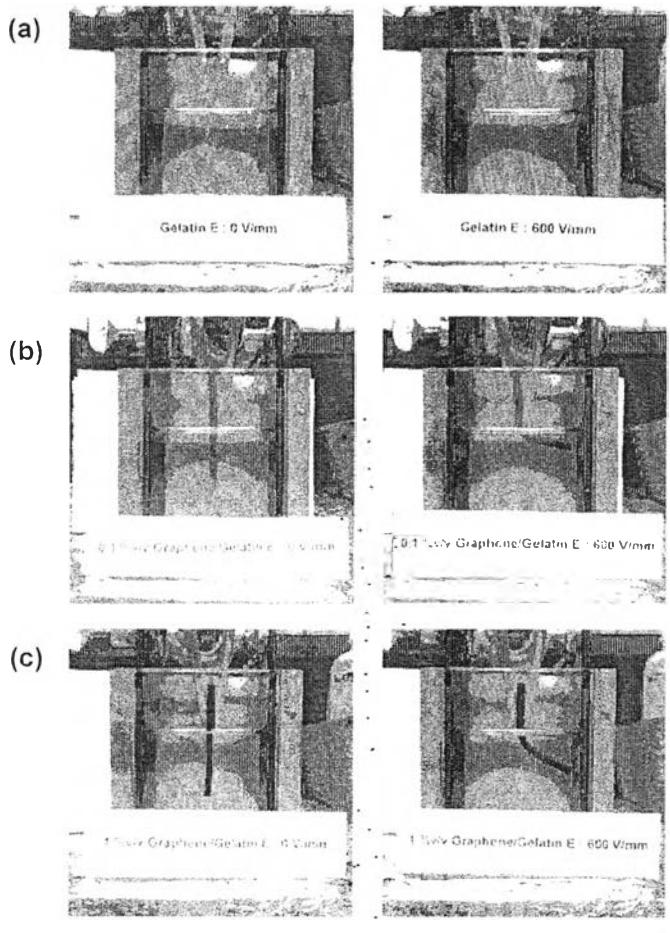

Figure 6.10 Deflection of the gelatin hydrogels at E = 0 and 600 V/mm: (a) pure gelatin hydrogel; (b) 0.1 vol% graphene/gelatin hydrogel; (c) 1 vol% graphene/gelatin hydrogel. (Note that the polarity of the electrode on the right-hand side is positive and the other is neutral)

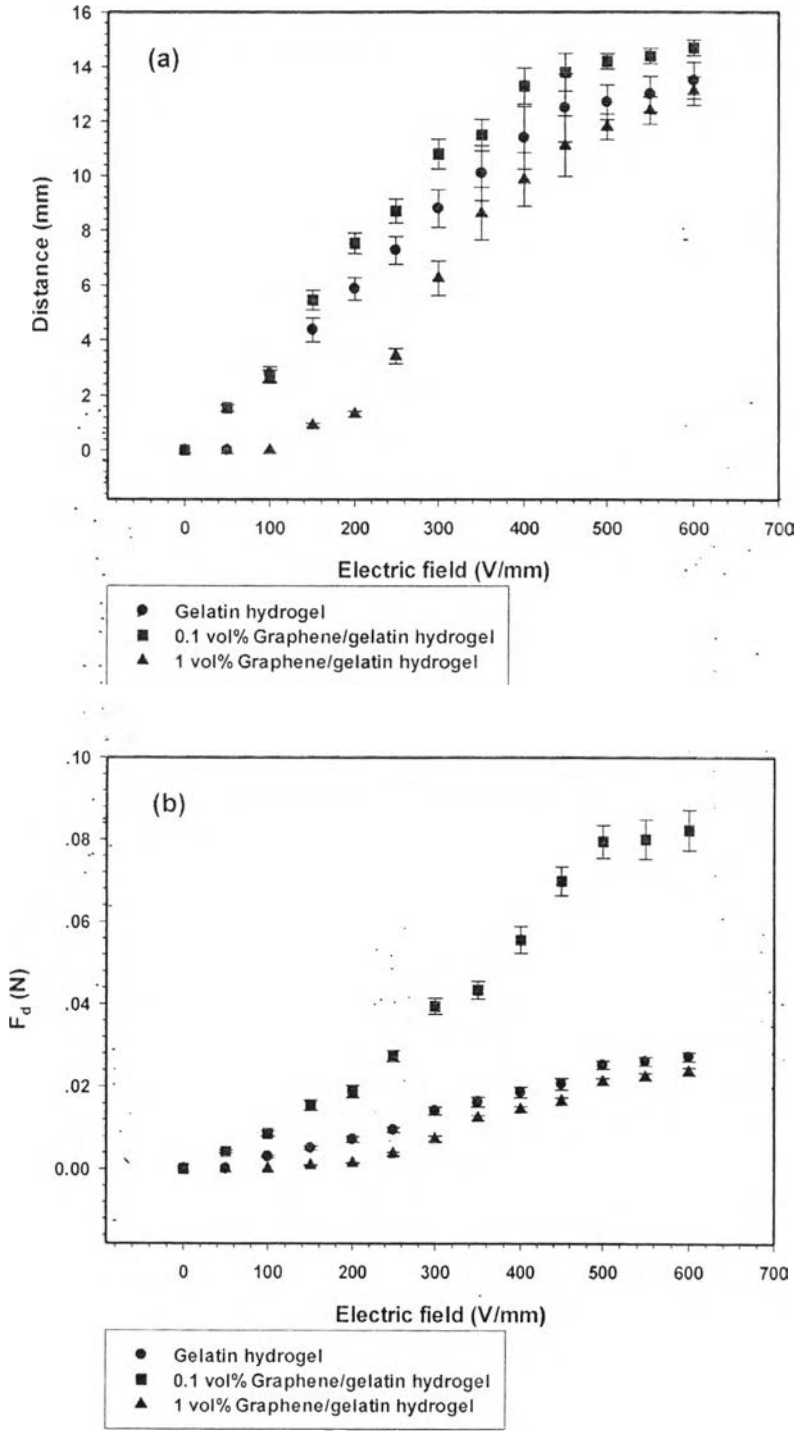

Figure 6.11 (a) Deflection distance of the pure gelatin hydrogel, the 0.1 vol% graphene/gelatin hydrogel, and the 1 vol% graphene/gelatin hydrogel at various electric field strengths. (b) Dielectropholetic force calculated through linear deflection theory.

Table 6.1 Determination of density, diameter, surface area, and conductivity of graphene

Sample	Graphene grade	Quoted diameter of Graphene (μm)	Measured diameter of graphene (μm)	Surface area (m^2/g)	Density (g/cm^3)	Average conductivity (S/cm)
Graphene	C (CG)	2	1.098 ± 0.22	40.58	2.140 ± 0.10	3065 ± 38
	M (MG)	15	12 ± 2.50	388.48	2.253 ± 0.12	15363 ± 393
	H (HG)	15	16 ± 2.13	114.55	2.202 ± 0.13	8701 ± 80

Table 6.2 Sensitivity of storage modulus of the pure gelatin hydrogel and the graphene/gelatin hydrogels (0.10 %strain, electric field strength 800 V/mm, frequency 100 rad/s, 30 °C)

Materials	Storage modulus (G′) (Pa)	Initial storage modulus (G_o') (Pa)	Sensitivity of storage modulus ($\Delta G'/ G_o'$)
Pure gelatin hydrogel	2.56×10^5	1.78×10^5	0.44
0.01 vol% MG/gelatin hydrogel	6.36×10^5	1.80×10^5	2.53
0.1 vol% MG/gelatin hydrogel	1.61×10^6	3.56×10^5	3.52
0.5 vol% MG/gelatin hydrogel	4.26×10^5	1.43×10^5	1.97
1 vol% MG/gelatin hydrogel	2.58×10^5	1.30×10^5	0.99

Table 6.3 Comparison of the storage modulus sensitivities ($\Delta G'/G'_o$) of electroactive and dielectric elastomer materials at temperature testing 27 °C

Materials	Electric field (V/mm)	Frequency (rad/s)	$\Delta G'/G'_o$	Ref
Polyesterurethane (LPR)	2000	100	2.080	Petcharoen *et al.*, 2013
Polyetherurethane (E95A)			1.560	
Styrene-isoprene-styrene triblock (D1114P)	1000	1	0.122	Thongsak *et al.*, 2010
Styrene-isoprene-styrene triblock (D1164P)			0.102	
Styrene-isoprene-styrene triblock (D1162P)			0.050	
Cellulose gel	1000	1	1.430	Kunchornsup *et al.*, 2012
Acrylic elastomer 70	1000	100	0.439	Kunanuruksapong *et al.*, 2008
Acrylic elastomer 71			0.586	
Acrylic elastomer 72			0.148	
Styrene-acrylic coolymer			1.195	
Acrylic elastomer 71 + 10 vol% PPP	2000	1	0.306	
Acrylic elastomer 71 + 30 vol% PPP			0.971	
Ethylene propylene diene elastomer (EPDM)	1000	100	0.300	Intanoo *et al.*, 2012
EPDM + 10 vol% PAZ			0.612	
EPDM + 20 vol% PAZ			1.125	